Acta Mech 233, 685–700 (2022)
https://doi.org/10.1007/s00707-021-03139-6

ORIGINAL PAPER

Mahmure Avey · A. H. Sofiyev · N. Kuruoglu

Influences of elastic foundations and thermal environments on the thermoelastic buckling of nanocomposite truncated conical shells

Received: 18 October 2021 / Revised: 11 December 2021 / Accepted: 24 December 2021 / Published online: 27 January 2022

Abstract In this study, the combined effects of two-parameter elastic foundation and thermal environment on the buckling behaviors of carbon nanotube (CNT) patterned composite conical shells in the framework of the shear deformation theory (SDT) are investigated. It is assumed that the nanocomposite conical shell is freely supported at its ends and that the material properties are temperature dependent. The derivation of fundamental equations of CNT-patterned truncated conical shells on elastic foundations is based on the Donnell shell theory. The Galerkin method is applied to the basic equations to find the expressions for the critical temperature (CT) and axial buckling loads of CNT-patterned truncated conical shells on elastic foundations and in thermal environments. In the presence of elastic foundations and thermal environments, it is estimated how the effects of CNT patterns, the volume fractions, and the characteristics of conical shells on the buckling load within SDT change by comparing them with the classical shell theory (CST).

1 Introduction

The rapid development of nanotechnology in recent years has facilitated the production of nanotubes and greatly expanded their applications. Carbon nanotubes produced by Iijima are used in various industries and are used in new materials with great potential for future use [1–3]. One of the most important applications for CNTs with superior properties is as a reinforcing element in conventional composites. The mechanical, thermal and electrical properties of composites reinforced with carbon nanotubes are significantly improved, and the resistance and strength of structural elements are also significantly increased [4–13]. These requirements increase the attention of researchers to the problems of stability of nanocomposite structures containing

M. Avey · A. H. Sofiyev
Information Technology Research and Application Center Member of Consultancy Board of ITRAC Center, Istanbul Commerce University, Beyoglu, 34445 Istanbul, Turkey
e-mail: mahmureavey@gmail.com

M. Avey
Analytical Information Resources Center of UNEC-Azerbaijan State Economic University, 1001 Baku, Azerbaijan

M. Avey
Division of Mathematics in Graduate Education Institute of Usak University, 64000 Usak, Turkey

A. H. Sofiyev (✉)
Department of Civil Engineering of Engineering Faculty of Suleyman Demirel University, 32260 Isparta, Turkey
e-mail: asofiyev@hotmail.com

A. H. Sofiyev
Scientific Research Centers for Composition Materials of UNEC-Azerbaijan State Economic University, 1001 Baku, Azerbaijan

N. Kuruoglu
Department of Civil Engineering, Faculty of Engineering and Architecture, Istanbul Gelisim University, 34315 Istanbul, Turkey
e-mail: nkuruoglu@gelisim.edu.tr

carbon nanotubes with smooth and inhomogeneous profiles under various loads and thermal environments. The stability of composite cylindrical shells reinforced with functionally graded CNTs in thermal environments was first discussed in the study by Shen [14]. After this study, some studies of the loss of stability of cylindrical and conical shells containing CNTs in thermal environments were carried out [15–21].

CNT-containing composites are increasingly used not only in the aerospace industry, but also in various engineering applications due to their many unique advantages, such as higher hardness and lighter weight, corrosion resistance and long service life compared to metals. Composite structures containing carbon nanotubes with a uniform and functional distribution are also used in civil and engineering construction, nuclear power plants, oil pipelines and other fields, so they come into contact with various types of soil. One such soil model is the Pasternak soil model or the two-parameter elastic foundation model [22]. A special case of this model is the well-known Winkler soil model, which consists of parallel springs that are not in contact with each other. Sun and Huang [23] adapted the Pasternak-type soil model for conical shells. With the help of these models, the behavior of the building element is investigated in various environments. When modeling structural elements containing carbon nanotubes, it is necessary to jointly investigate the influence of an elastic foundation, thermal environment, and reinforcement on the buckling load, which makes materials functionally differentiated. In the literature, there are some studies on the interaction of structural elements containing CNTs with soil in thermal environments, and most of those used cylindrical shells and panels or used numerical methods [24–30].

Since the volumetric content of composites reinforced with carbon nanotubes is distributed as a gradient, the transverse shear modulus of the construction is much lower than the effective elastic modulus in the direction of the fiber, it is more susceptible to transverse shear, and should be considered. These factors necessitate generalization of the previously known shear deformation theories [31–34] to the problems of CNT reinforced structural elements. The application of shear deformation theory to the thermal stability problems of conical shells composed of functionally graded materials was first performed by Sofiyev [35].

A review of the literature shows that the stability characteristics of polymer conical shells with CNT patterns resting on a two-parameter elastic foundation within SDT have not been sufficiently studied in the thermal environment. The aim of present study will be to eliminate this deficiency.

2 Theoretical development

Consider that a truncated conical shell with slant length l, thickness h, small and large bases circle radii b and a, and half-peak angle α made of polymer with a CNT pattern is resting on the elastic foundation, which uses a two-parameter elastic foundation model proposed by Pasternak [22] and developed by Sun and Huang [23] for conical shells (Fig. 1). In this model, the pressure on the bottom surface of the cone is expressed by the following expression [23]:

$$N = K_w w - K_p \left(\frac{\partial^2 w}{\partial S^2} + \frac{1}{S}\frac{\partial w}{\partial S} + \frac{1}{S^2}\frac{\partial^2 w}{\partial \theta_1^2} \right) \tag{1}$$

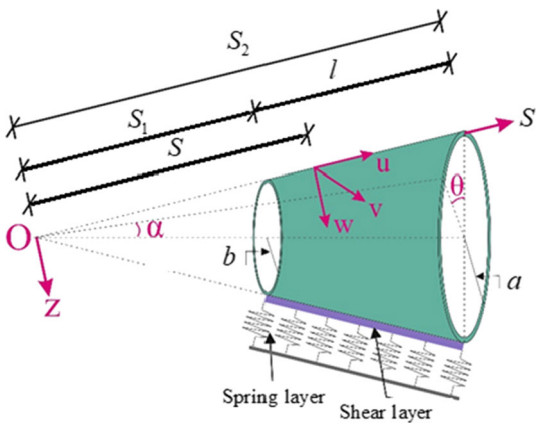

Fig. 1 Truncated conical shell made of polymer with the CNT pattern on an elastic foundation

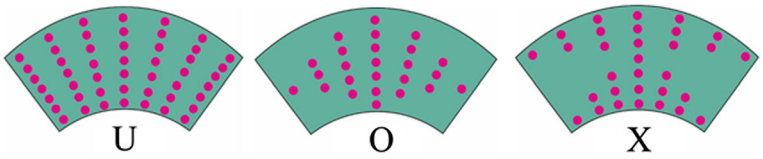

Fig. 2 CNT distribution throughout the thickness of the polymer cone

where $\theta_1 = \theta \sin\alpha$, N is the surface pressure, and K_w and K_p are the normal elastic modulus and shear modulus of the foundation, namely the Winkler foundation parameter and the Pasternak foundation parameter.

The truncated conical shell is referenced to a coordinate system ($O\ S\theta z$) in which S and θ are along the meridional and circumferential directions of the cone and z is in the direction of the inward normal to the reference surface. The displacements corresponding to the coordinate axes are denoted by u, v, and w, and the rotations of the normal to the reference surface are denoted by χ_1 and χ_2 with respect to θ and S, respectively.

It was easily obtained in the practice by Kwon et al. [13] that the material properties of functionally graded nanocomposites are linear functions of the volume fraction of CNTs through the thickness. As in Shen [14], uniform (U) and three shapes of V-, O-, and X-patterns can be considered:

$$V_{cnt}(z_1) = \begin{cases} V^*_{cnt} & \text{for } U \text{ pattern} \\ (1+2z_1)V^*_{cnt} & \text{for } O \text{ pattern} \\ 4|z_1|V^*_{cnt} & \text{for } X \text{ pattern} \end{cases} \tag{2}$$

where $z_1 = z/h$ and the following definition applies:

$$V^*_{cnt} = m_{cnt}/[m_{cnt}(1-\rho_{cnt}/\rho_m) + \rho_{cnt}/\rho_m] \tag{3}$$

in which m_{cn} is a mass fraction of CNTs. The CNT distribution throughout the thickness of the polymer cone is shown in Fig. 2.

We assume that the material properties of CNTs and polymer are temperature dependent [14]:

$$E_{11}(z_1,T) = \eta_1 V_{cnt}(z_1)E^{cnt}_{11}(T) + V^m E^m,\ \frac{\eta_2}{E_{22}(z_1,T)} = \frac{V_{cnt}(z_1)}{E^{cnt}_{22}(T)} + \frac{V^m}{E^m(T)},\ \frac{\eta_3}{G_{12}(z_1)} = \frac{V_{cnt}(z_1)}{G^{cnt}_{12}(T)} + \frac{V^m}{G^m(T)},$$
$$G_{13}(z_1,T) = G_{12}(z_1,T),\ G_{23}(z_1,T) = 1.2G_{12}(z_1,T),\ \nu_{12} = V^*_{cnt}\nu^{cnt}_{11} + V^m\nu^m,$$
$$\rho = V^*_{cnt}\rho^{cnt} + V^m\rho^m,\ V^{cnt}(z_1) + V_m = 1 \tag{4}$$

where V represents the volume fraction, superscript CNT and m represent the corresponding property for CNT and matrix, respectively, the efficiency parameters are indicated by $\eta_i (i = 1, 2, 3)$, and the elasticity moduli and Poisson's ratios of the polymer (or matrix) and CNTs are denoted by $E^m(T)$, ν^m and $E^{cnt}_{kk}(T)$, $(k = 1, 2)$, $G^{cnt}_{12}(T)$, ν^{cnt}_{12}, respectively.

The thermal expansion coefficients in the S and θ directions are given by [14]

$$\alpha_{11}(z_1,T) = \frac{\alpha^{cn}_{11}(T)V_{cnt}(z_1)E^{cn}_{11}(T) + V^m E^m(T)\alpha^m(T)}{V_{cnt}(z_1)E^{cn}_{11}(T) + V^m E^m(T)},$$
$$\alpha_{22}(z_1,T) = (1+\nu^{cnt}_{12})\alpha^{cnt}_{22}(T)V_{cnt}(z_1) + (1+\nu^m)V^m\alpha^m(T) - \nu_{12}\alpha_{11}(z_1,T) \tag{5}$$

where $\alpha^{cnt}_{11}(T)$, $\alpha^{cnt}_{22}(T)$, and $\alpha^m(T)$ are thermal expansion coefficients.

In the framework of SDT [31], considering the cone-foundation interaction and thermal effects, the governing equations of CNT-patterned conical shells [36, 37] can be derived in terms of w, χ_1, χ_2, and the stress function F, defined by the relations

$$(T_S, T_\theta, T_{S\theta}) = h\left(\frac{1}{S^2}\frac{\partial^2 F}{\partial\theta_1^2} + \frac{1}{S}\frac{\partial F}{\partial S}, \frac{\partial^2 F}{\partial S^2}, -\frac{1}{S}\frac{\partial^2 F}{\partial S\partial\theta_1} + \frac{1}{S^2}\frac{\partial F}{\partial\theta_1}\right). \tag{6}$$

The basic equations can be expressed as (See, Appendix 1)

$$h\left[c_{12}\frac{\partial^4 F}{\partial S^4} + \frac{c_{11}-c_{31}}{S^2}\frac{\partial^4 F}{\partial S^2\partial\theta_1^2} + \frac{3c_{31}-c_{21}-3c_{11}}{S^3}\frac{\partial^3 F}{\partial S\partial\theta_1^2} + \frac{c_{11}+c_{12}-c_{22}}{S}\frac{\partial^3 F}{\partial S^3} + \frac{2c_{21}}{S^3}\frac{\partial F}{\partial S}\right.$$

$$+\frac{c_{22}-c_{12}-c_{11}-c_{21}}{S^2}\frac{\partial^2 F}{\partial S^2}+\frac{3(c_{21}+c_{11}-c_{31})}{S^4}\frac{\partial^2 F}{\partial\theta_1^2}\Bigg]-c_{13}\frac{\partial^4 w}{\partial S^4}+\frac{3c_{14}+3c_{32}+c_{24}}{S^3}\frac{\partial^3 w}{\partial S\partial\theta_1^2}$$
$$-\frac{c_{14}+c_{32}}{S^2}\frac{\partial^4 w}{\partial S^2\partial\theta_1^2}-\frac{c_{13}+c_{14}-c_{23}}{S}\frac{\partial^3 w}{\partial S^3}+\frac{c_{13}+c_{14}-c_{23}+c_{24}}{S^2}\frac{\partial^2 w}{\partial S^2}-\frac{3(c_{14}+c_{24}+c_{32})}{S^4}\frac{\partial^2 w}{\partial\theta_1^2}$$
$$-\frac{2c_{24}}{S^3}\frac{\partial w}{\partial S}+c_{15}\frac{\partial^3\chi_1}{\partial S^3}+\frac{c_{15}-c_{25}}{S}\frac{\partial^2\chi_1}{\partial S^2}+\frac{c_{35}}{S^2}\frac{\partial^3\chi_1}{\partial S\partial\theta_1^2}-I_3\frac{\partial\chi_1}{\partial S}-\frac{c_{15}-c_{25}}{S^2}\frac{\partial\chi_1}{\partial S}-\frac{c_{35}}{S^3}\frac{\partial^2\chi_1}{\partial\theta_1^2}$$
$$+\frac{c_{38}+c_{18}}{S}\frac{\partial^3\chi_2}{\partial S^2\partial\theta_1}-\frac{c_{28}+c_{18}+c_{38}}{S^2}\frac{\partial^2\chi_2}{\partial S\partial\theta_1}+\frac{2c_{28}}{S^3}\frac{\partial\chi_2}{\partial\theta_1}=0, \tag{7}$$

$$h\Bigg[\frac{c_{21}}{S^3}\frac{\partial^4 F}{\partial\theta_1^4}+\frac{c_{22}-c_{31}}{S}\frac{\partial^4 F}{\partial S^2\partial\theta_1^2}+\frac{c_{21}}{S^2}\frac{\partial^3 F}{\partial S\partial\theta_1^2}\Bigg]-\frac{c_{32}+c_{23}}{S}\frac{\partial^4 w}{\partial S^2\partial\theta_1^2}-\frac{c_{24}}{S^2}\frac{\partial^3 w}{\partial S\partial\theta_1^2}-\frac{c_{24}}{S^3}\frac{\partial^4 w}{\partial\theta_1^4}$$
$$+\frac{c_{25}+c_{35}}{S}\frac{\partial^3\chi_1}{\partial S\partial\theta_1^2}+\frac{c_{35}}{S^2}\frac{\partial^2\chi_1}{\partial\theta_1^2}+c_{38}\frac{\partial^3\chi_2}{\partial S^2\partial\theta_1}+\frac{2c_{38}}{S}\frac{\partial^2\chi_2}{\partial S\partial\theta_1}+\frac{c_{28}}{S^2}\frac{\partial^3\chi_2}{\partial\theta_1^3}-I_4\frac{\partial\chi_2}{\partial\theta_1}=0, \tag{8}$$

$$h\Bigg[\frac{b_{11}}{S^4}\frac{\partial^4 F}{\partial\theta_1^4}+\frac{2b_{31}+b_{21}+b_{12}}{S^2}\frac{\partial^4 F}{\partial S^2\partial\theta_1^2}-\frac{2(b_{31}+b_{21})}{S^3}\frac{\partial^3 F}{\partial S\partial\theta_1^2}+\frac{2(b_{31}+b_{21}+b_{11})}{S^4}\frac{\partial^2 F}{\partial\theta_1^2}+\frac{b_{11}}{S^3}\frac{\partial F}{\partial S}$$
$$-\frac{b_{11}}{S^2}\frac{\partial^2 F}{\partial S^2}+\frac{b_{21}+2b_{22}-b_{12}}{S}\frac{\partial^3 F}{\partial S^3}+b_{22}\frac{\partial^4 F}{\partial S^4}\Bigg]$$
$$-\frac{b_{14}}{S^4}\frac{\partial^4 w}{\partial\theta_1^4}+\frac{2b_{32}-b_{13}-b_{24}}{S^2}\frac{\partial^4 w}{\partial S^2\partial\theta_1^2}+\frac{2(b_{24}-b_{32})}{S^3}\frac{\partial^3 w}{\partial S\partial\theta_1^2}-\frac{b_{14}}{S^3}\frac{\partial w}{\partial S}$$
$$+\frac{2(b_{32}-b_{24}-b_{14})}{S^4}\frac{\partial^2 w}{\partial\theta_1^2}+\left(\frac{b_{14}}{S^2}+\frac{1}{S\tan\alpha}\right)\frac{\partial^2 w}{\partial S^2}+\frac{b_{13}-b_{24}-2b_{23}}{S}\frac{\partial^3 w}{\partial S^3}-b_{23}\frac{\partial^4 w}{\partial S^4}+\frac{2b_{35}+b_{15}}{S^2}\frac{\partial^3\chi_1}{\partial S\partial\theta_1^2}$$
$$+b_{25}\frac{\partial^3\chi_1}{\partial S^3}+\frac{2b_{25}-b_{15}}{S}\frac{\partial^2\chi_1}{\partial S^2}+\frac{b_{18}}{S^3}\frac{\partial^3\chi_2}{\partial\theta_1^3}+\frac{2b_{38}+b_{28}}{S}\frac{\partial^3\chi_2}{\partial S^2\partial\theta_1}+\frac{2b_{38}-b_{18}}{S^2}\frac{\partial^2\chi_2}{\partial S\partial\theta_1}+\frac{b_{18}}{S^3}\frac{\partial\chi_2}{\partial\theta_1}=0 \tag{9}$$

$$\frac{h}{S\tan\alpha}\frac{\partial^2 F}{\partial S^2}+T_S^0\frac{\partial^2 w}{\partial S^2}-K_w w-K_p\left(\frac{\partial^2 w}{\partial S^2}+\frac{1}{S}\frac{\partial w}{\partial S}+\frac{1}{S^2}\frac{\partial^2 w}{\partial\theta_1^2}\right)+I_3\left(\frac{\partial\chi_1}{\partial S}+\frac{\chi_1}{S}\right)+\frac{I_4}{S}\frac{\partial\chi_2}{\partial\theta_1}=0 \tag{10}$$

where T_S^0 is the pre buckling force, $I_k(k=3,4)$, and b_{ij} and c_{ij} $(i=1,2,3,\ j=1,2,\ldots 8)$ are the temperature-dependent parameters given in Appendix 2. It should be noted that in the set of Eqs. (7)–(10) the thermal moment due to the temperature gradient along the wall thickness is not considered.

In the next step, two different boundary-value problems will be discussed.

a. The material properties of nanocomposite cylindrical shells are independent of temperature and are under the thermal load. In this case, the membrane form of the equilibrium equations turns into the following expressions [25]:

$$T_S^0=-\Pi=-\int_{-h/2}^{h/2}\lfloor H_{11}(z_1,T)\alpha_{11}(z_1,T)+H_{12}(z_1,T)\alpha_{22}(z_1,T)\rfloor\Delta T\,dz,\quad T_\theta^0=0,\quad T_{S\theta}^0=0, \tag{11}$$

b. The material properties of nanocomposite cylindrical shells are dependent of temperature and under axial compressive load. In this case, the membrane form of the equilibrium equations turns into the following expressions [25]:

$$T_S^0=-T,\quad T_\theta^0=0,\quad T_{S\theta}^0=0 \tag{12}$$

where Π is the thermal parameter, T is the axial compressive load, and $\Delta T=T_1-T_0$ is the temperature rise from a certain reference temperature T_0, at which there are no thermal strains, and $H_{ij}(i,\ j=1,2)$ are defined in Appendix 1.

3 Solution method

For the freely supported ends, the coordinates of the conical shell are transformed from (S, θ_1) to (x, θ_1) by the following relation: $x = \ln(S/S_2)$. Considering this transformation, the approximation functions for the solution of the fundamental equations of CNT-reinforced conical shells satisfying the freely supported boundary conditions can be sought as follows [35]:

$$\begin{aligned} F &= A_1 S_2\, e^{(\xi+1)x} \sin(\beta_1 x)\cos(\beta_2\theta_1), \quad w = A_2 e^{\xi x}\sin(\beta_1 x)\cos(\beta_2\theta_1), \\ \chi_1 &= A_3 e^{\xi x}\cos(\beta_1 x)\cos(\beta_2\theta_1), \quad \chi_2 = A_4 e^{\xi x}\sin(\beta_1 x)\sin(\beta_2\theta_1), \end{aligned} \tag{13}$$

where $A_i (i = 1, 2, \ldots, 4)$ are unknown amplitudes, $\beta_1 = \frac{m\pi}{x_0}$ and $\beta_2 = \frac{n}{\sin\theta}$ in which $(m,\ n)$ is the buckling mode, $x_0 = \ln\frac{S_1}{S_2}$, and ξ is the unknown parameter which determined the minimum conditions of the critical temperature and axial buckling load.

After placing the approximate functions (13) into the system of Eqs. (7)–(11), the determinant of the matrix consisting of coefficients of the algebraic equations obtained after the application of the Galerkin method is set to zero, and the following expression is obtained for the critical temperature of CNT-patterned cones on elastic foundations within SDT:

$$T_{sdt}^{Tbucwp} = \frac{u_{41}\vartheta_1 + u_{43}\vartheta_3 + u_{44}\vartheta_4 + \vartheta_2(u_W + u_P)}{\Pi_0\vartheta_2 u_T} \tag{14}$$

where

$$\Pi_0 = \int_{-h/2}^{h/2} \lfloor H_{11}(z_1, T)\alpha_{11}(z_1, T) + H_{12}(z_1, T)\alpha_{22}(z_1, T)\rfloor \mathrm{d}z, \tag{15}$$

$$\vartheta_1 = -\begin{vmatrix} u_{12} & u_{13} & u_{14} \\ u_{22} & u_{23} & u_{24} \\ u_{32} & u_{33} & u_{34} \end{vmatrix},\ \vartheta_2 = \begin{vmatrix} u_{11} & u_{13} & u_{14} \\ u_{21} & u_{23} & u_{24} \\ u_{31} & u_{33} & u_{34} \end{vmatrix},\ \vartheta_3 = -\begin{vmatrix} u_{11} & u_{12} & u_{14} \\ u_{21} & u_{22} & u_{24} \\ u_{31} & u_{32} & u_{34} \end{vmatrix},\ \vartheta_4 = \begin{vmatrix} u_{11} & u_{12} & u_{13} \\ u_{21} & u_{22} & u_{23} \\ u_{31} & u_{32} & u_{33} \end{vmatrix} \tag{16}$$

in which the details of the coefficients $u_{ij}(i, j = 1, 2, ..., 4)$ and u_T, u_w, u_P are given in Appendix 2. In expression (14), the material properties of the nanocomposites are independent of temperature.

Considering (12) instead of (11), the following expression is obtained for the axial buckling load of CNT-patterned conical shells on elastic foundations and in the thermal environment:

$$T_{sdt}^{axbucwp} = \frac{u_{41}\vartheta_1 + u_{43}\vartheta_3 + u_{44}\vartheta_4 + \vartheta_2(u_W + u_P)}{\vartheta_2 u_T E^m h}. \tag{17}$$

The nondimensional axial buckling load (NABL) of CNT-patterned conical shells resting on elastic foundations and in the thermal environment is defined as:

$$T_{1sdt}^{axbucwp} = \frac{T_{sdt}^{axbucwp}}{E^m h}. \tag{18}$$

Assuming that the unit normal is perpendicular to the mid-surface before and after deformation, the expressions (14) and (18) transform into the expressions for CT and NABL of CNT-patterned conical shells on elastic foundations based on the CST and are denoted as T_{cst}^{Tbucwp} and $T_{cst}^{axbucwp}$, respectively, in the special cases.

When the half apex-angle approaches zero ($\alpha \to 0$), the expressions for CT and NABL of CNT-patterned cylindrical shells on elastic foundations based on the SDT are obtained from expressions (14) and (18), respectively, in the special cases.

When K_w and K_p in the expressions (14) and (18) are considered equal to zero at the same time, the expressions for CT and NABL of unconstrained conical shells by CNT patterns are obtained in the special cases.

The minimum values of CT and NABL for nanocomposite cones on elastic foundations in the framework of STD are found by minimizing (14) and (18) depending on the parameters *m, n,* and ξ. The minimum values of CT and NABL for freely supported nanocomposite cones in the framework of STD and CST are achieved at approximately $\xi = 2.1$.

Table 1 Comparison of the axial buckling load of cylindrical shells with U- and X-patterns within SDT in thermal environments

	$T_{Shen}^{axbucsdt} = 2\pi R_{cyl} T_{sdt}^{axbuc}$ (in kN), (m, n)			
T(K)	U Shen [14]	X	U Present study	X
300	122.25	148.06	122.026 (2,4)	148.958 (1,3)
500	97.56	113.56	97.739 (2,4)	113.021 (1,3)
700	68.96	76.49	69.910 (1,3)	76.185 (1,3)

4 Numerical results and discussion

4.1 Comparison studies

The magnitudes of the axial buckling load of unconstrained shear deformable cylindrical shells modeled with U- and X-type CNTs are listed in Table 1 for comparison with the results of Shen [14] in thermal environments. Since the axial buckling load in the thermal environment is used as $T_{Shen}^{axbucsdt} = 2\pi R_{cyl} T_{sdt}^{axbuc}$ in Ref. [14], the expression (17) in our study is multiplied by $2\pi R_{cyl}$ at $K_w = K_p = 0$, $\alpha \to 0°$. In comparison, poly (methyl methacrylate) called PMMA is chosen for the matrix and (10, 10) CNTs as reinforcement. The material properties of PMMA are: $Y^m(T) = (3.52 - 0.0034T)$ GPa, $\nu^m = 0.34$, $\alpha^m(T) = 45(1 + 0.0005\Delta T) \times 10^{-6}$/K, where $T = T_0 + \Delta T$ and $T = 300$ K (room temperature). In such a way, $\alpha^m = 45 \times 10^{-6}$/K, $Y^m = 2.5$ GPa at $T = 300$ K. The posteriori specified shape functions are defined as: $f_i(z) = z - \frac{4}{3}z^3$, $(i = 1, 2)$ [31]. The variation of the thermomechanical properties of CNT with temperature is expressed by the following cubic functions [14]:

$$E_{11}^{cnt}(T) = (6.3998 - 4.338417 \times 10^{-3} \times T + 7.43 \times 10^{-6} \times T^2 - 4.458333 \times 10^{-9} \times T^3) \times 10^{12},$$
$$E_{22}^{cnt}(T) = (8.02155 - 5.420375 \times 10^{-3} \times T + 9.275 \times 10^{-6} \times T^2 - 5.5625 \times 10^{-9} \times T^3) \times 10^{12},$$
$$G_{12}^{cnt}(T) = (1.4075 + 3.476208 \times 10^{-3} \times T - 6.965 \times 10^{-6} \times T^2 + 4.479167 \times 10^{-9} \times T^3) \times 10^{12},$$
$$\alpha_{11}^{cnt}(T) = (-1.12515 + 0.02291688 \times T - 2.887 \times 10^{-5} \times T^2 + 1.13625 \times 10^{-8} \times T^3) \times 10^{-6},$$
$$\alpha_{22}^{cnt}(T) = (5.43715 - 9.984625 \times 10^{-4} \times T + 2.9 \times 10^{-7} \times T^2 + 1.25 \times 10^{-11} \times T^3) \times 10^{-6}.$$

The efficiency parameters are given as [13]:

$$\eta_1 = 0.137,\ \eta_2 = 1.022,\ \eta_3 = 0.7\eta_2 \ \text{ at } \ V_{cnt}^* = 0.12;\ \eta_1 = 0.142,\ \eta_2 = 1.626,\ \eta_3 = 0.7\eta_2 \ \text{ at } \ V_{cnt}^* = 0.17;$$
$$\eta_1 = 0.141,\ \eta_2 = 1.585,\ \eta_3 = 0.7\eta_2 \ \text{ at } \ V_{cnt}^* = 0.28.$$

The geometrical characteristics of CNT and cylinders are: $L_{cnt} = 9.26$ nm, $R_{cnt} = 0.68$ nm, $h_{cnt} = 0.067$ nm, $\nu_{12}^{cnt} = 0.175$, and $R_{cyl} = 0.06$(m), $h = 0.002$ (m), $l_{cyl} = 0.1987$(m), $V_{cnt}^* = 0.17$ [14].

As can be seen from Table 1, the minimum values of the axial buckling load of the U and X-patterned CNT cylindrical shells within SDT obtained in our study at $T = 300$, 500, and 700 (K) are in very good agreement with the results of Shen [14]. The numbers in parentheses (m, n) are the wave numbers corresponding to the minimum values of the axial buckling load in thermal environments. The minimum value of axial compressive buckling load for cylindrical shells is obtained at $\xi = 0$.

4.2 Thermo-elastic buckling analysis

In this Subsection, numerical results are presented for CNT-patterned conical shells exposed to uniform temperature or axial compressive load. For specific analyses, PMMA as matrix and (10, 10) SWCNTs as reinforcement were chosen, whose material properties were presented in the previous comparison. The following symbols are used as $T_{1cst}^{Tbucwp} = T_{cst}^{Tbucwp}/10^3$, $T_{1sdt}^{Tbucwp} = T_{sdt}^{Tbucwp}/10^3$, $\overline{T}_{1cst}^{axbucwp} = 10T_{1cst}^{axbucwp}$ and $\overline{T}_{1sdt}^{axbucwp} = 10T_{1sdt}^{axbucwp}$.

The variation of the values of the critical temperature and corresponding modes (m, n) of CNT-patterned cones with the material properties independent of temperature versus the coefficients of two-parameter soil

Table 2 Variation of the minimum values of the critical temperature and corresponding thermal buckling modes (m, n) versus the K_w(in N/m^3) and K_p (in N/m)

		$\overline{K}_w = K_w/10^8,\ \overline{K}_P = K_P/10^4$					
$\overline{K}_w$	$\overline{K}_p$	T_{1cst}^{Tcrwp} (m, n) U	T_{1sdt}^{Tcrwp} (m, n)	T_{1cst}^{Tcrwp} (m, n) O	T_{1sdt}^{Tcrwp} (m, n)	T_{1cst}^{Tcrwp} (m, n) X	T_{1sdt}^{Tcrwp} (m, n)
0	0	0.587 (1,4)	0.486 (1,4)	0.432 (1,4)	0.366 (1,4)	0.811 (1,4)	0.602 (1,5)
1.5	0	0.617 (1,4)	0.517 (1,4)	0.463 (1,4)	0.396 (1,4)	0.841 (1,4)	0.632 (1,5)
	2	0.670 (1,4)	0.570 (1,4)	0.515 (1,4)	0.449 (1,4)	0.894 (1,4)	0.688 (1,4)
	2.25	0.677 (1,4)	0.576 (1,4)	0.522 (1,4)	0.456 (1,4)	0.900 (1,4)	0.694 (1,4)
	2.5	0.683 (1,4)	0.583 (1,4)	0.528 (1,4)	0.462 (1,4)	0.907 (1,4)	0.701 (1,4)
	2.75	0.690 (1,4)	0.589 (1,4)	0.535 (1,4)	0.469 (1,4)	0.913 (1,4)	0.708 (1,4)
1.75	0	0.622 (1,4)	0.522 (1,4)	0.468 (1,4)	0.401 (1,4)	0.846 (1,4)	0.638 (1,5)
	2	0.675 (1,4)	0.575 (1,4)	0.520 (1,4)	0.454 (1,4)	0.899 (1,4)	0.693 (1,4)
	2.25	0.682 (1,4)	0.581 (1,4)	0.527 (1,4)	0.461 (1,4)	0.905 (1,4)	0.699 (1,4)
	2.5	0.688 (1,4)	0.588 (1,4)	0.533 (1,4)	0.467 (1,4)	0.912 (1,4)	0.706 (1,4)
	2.75	0.695 (1,4)	0.595 (1,4)	0.540 (1,4)	0.474 (1,4)	0.919 (1,4)	0.713 (1,4)
2	0	0.627 (1,4)	0.527 (1,4)	0.473 (1,4)	0.406 (1,4)	0.851 (1,4)	0.643 (1,5)
	2	0.680 (1,4)	0.580 (1,4)	0.525 (1,4)	0.459 (1,4)	0.904 (1,4)	0.698 (1,4)
	2.25	0.687 (1,4)	0.586 (1,4)	0.532 (1,4)	0.466 (1,4)	0.910 (1,4)	0.704 (1,4)
	2.5	0.694 (1,4)	0.593 (1,4)	0.539 (1,4)	0.472 (1,4)	0.917 (1,4)	0.711 (1,4)
	2.75	0.700 (1,4)	0.600 (1,4)	0.545 (1,4)	0.479 (1,4)	0.924 (1,4)	0.718 (1,4)
2.25	0	0.633 (1,4)	0.532 (1,4)	0.478 (1,4)	0.411 (1,4)	0.856 (1,4)	0.648 (1,5)
	2	0.685 (1,4)	0.585 (1,4)	0.530 (1,4)	0.464 (1,4)	0.909 (1,4)	0.703 (1,4)
	2.25	0.692 (1,4)	0.591 (1,4)	0.537 (1,4)	0.471 (1,4)	0.915 (1,4)	0.710 (1,4)
	2.5	0.699 (1,4)	0.598 (1,4)	0.544 (1,4)	0.477 (1,4)	0.922 (1,4)	0.716 (1,4)
	2.75	0.705 (1,4)	0.605 (1,4)	0.550 (1,4)	0.484 (1,4)	0.929 (1,4)	0.723 (1,4)

K_w, and K_P are presented in Table 2. As can be seen from Table 2, the values of the CT increase as the soil coefficients K_w(in N/m^3) and K_p (in N/m) increase separately and together. The following data are used: $T = 300\,(\mathrm{K}),\ l/b = 1,\ b/h = 20,\ \alpha = 25°,\ V_{cnt}^* = 0.12,\ h = 0.002\mathrm{m},\ \overline{K}_w = K_w/10^8,\ \overline{K}_P = K_P/10^4$. In the presence of ground, the effect of transverse shear deformations (TSDs) on the critical temperature is reduced compared to unconstrained CNT-patterned conical shells. While TSDs effect decreases more slowly for the Winkler foundation or $K_w \neq 0,\ K_p = 0$, this decrease is more pronounced for the Pasternak foundation or $(K_w, K_p) \neq (0, 0)$. For example, excluding the influence of the foundation, i.e., $(K_w, K_p) = (0, 0)$, the effects of TSDs on the CT are 17.21%, 15.28% and 25.77% for composite conical shells with U-, O- and X-patterns, respectively, while if $(K_w, K_p) = (1.5 \times 10^8, 0)$, those effects are slightly reduced for each of the templates U, O, and X and are, respectively, 16.21%, 14.47%, and 24.85%, and if $(K_w, K_p) = (2.25 \times 10^8,\ 2.75 \times 10^4)$, those effects are 14.18%, 12%, and 22.17%, respectively.

In the presence of ground, the effect of templates on the CT is reduced compared to unconstrained CNT-patterned conical shells. While it decreases slowly for $K_w \neq 0,\ K_p = 0$, this decrease is more pronounced for $(K_w, K_p) \neq (0, 0)$. For example, excluding the influence of the foundation, i.e., $(K_w, K_p) = (0, 0)$, the effects of O- and X-templates on the CT are (− 24.69%) and (+ 23.87%), respectively, while those effects are slightly reduced for each of O- and X-templates and are, respectively, (− 23.4%) and (+ 22.4%), if $(K_w, K_p) = (1.5 \times 10^8, 0)$, moreover those effects are (− 20%) and (+ 19.5%), respectively, if $(K_w, K_p) = (2.25 \times 10^8,\ 2.75 \times 10^4)$. In the presence of Pasternak and Winkler foundations, TSDs reduce the influence of the O-shape on the critical temperature by about 1.5–2% compared to the CST, while in the X-shape it is reduced by about 12–15%.

Tables 3 and 4 and Figs. 3 and 4 show the changes of the nondimensional axial buckling load of CNT-patterned truncated conical shells in the presence and absence of elastic foundations in thermal environments depending on the increase of the half-peak angle α based on SDT and CST. The following data are used in the creation of Tables 3 and 4, and Figs. 3 and 4: $l = b,\ b = 20h,\ V_{cnt}^* = 0.12,\ h = 2(\mathrm{mm}),\ K_w = 1.5 \times 10^8(\mathrm{N/m^3}),\ K_p = 2.75 \times 10^4(\mathrm{N/m}), T = 300, 400, 500,$ and 600 (K). In the framework of both theories, as the α increases from 10° to 45°, the magnitudes of the NABL of nanocomposite conical shells with and without elastic foundations decrease, while this decrease becomes more pronounced with the increasing of the temperature.

Table 3 Variation of the magnitudes of $T_{1cst}^{axbucwp}$, $T_{1sdt}^{axbucwp}$ and corresponding axial buckling modes for CNT-patterned cones on the elastic foundation in thermal environments versus the angle α

α	$\overline{T}_{1cst}^{axbucwp}(m,n)$ U	$\overline{T}_{1sdt}^{axbucwp}(m,n)$	$\overline{T}_{1cst}^{axbucwp}(m,n)$ O	$\overline{T}_{1sdt}^{axbucwp}(m,n)$	$\overline{T}_{1cst}^{axbucwp}(m,n)$ X	$\overline{T}_{1sdt}^{axbucwp}(m,n)$
$T = 300$ (K), $K_w = 1.5 \times 10^8$(N/m^3), $K_p = 2.75 \times 10^4$(N/m)						
10°	1.202 (1,4)	1.004 (1,4)	0.941 (1,4)	0.809 (1,4)	1.583 (1,4)	1.195 (1,4)
20°	1.122 (1,4)	0.948 (1,4)	0.874 (1,4)	0.759 (1,4)	1.486 (1,4)	1.136 (1,4)
30°	1.038 (1,4)	0.899 (1,4)	0.805 (1,4)	0.713 (1,4)	1.381 (1,4)	1.086 (1,4)
40°	0.957 (1,4)	0.853 (1,4)	0.738 (1,4)	0.670 (1,4)	1.280 (1,4)	1.041 (1,4)
45°	0.918 (1,4)	0.832 (1,4)	0.707 (1,4)	0.650 (1,4)	1.233 (1,4)	1.020 (1,4)
$T = 400$ (K)						
10°	1.154 (1,4)	0.942 (1,4)	0.898 (1,4)	0.764 (1,4)	1.526 (1,3)	1.116 (1,4)
20°	1.080 (1,4)	0.892 (1,4)	0.836 (1,4)	0.719 (1,4)	1.438 (1,4)	1.064 (1,4)
30°	1.001 (1,4)	0.848 (1,4)	0.772 (1,4)	0.677 (1,4)	1.339 (1,4)	1.020 (1,4)
40°	0.925 (1,4)	0.808 (1,4)	0.710 (1,4)	0.639 (1,4)	1.244 (1,4)	0.981 (1,4)
45°	0.888 (1,4)	0.789 (1,4)	0.682 (1,4)	0.621 (1,4)	1.197 (1,3)	0.962 (1,4)
$T = 500$ (K)						
10°	1.107 (1,3)	0.879 (1,4)	0.859 (1,4)	0.719 (1,4)	1.476 (1,3)	1.034 (1,4)
20°	1.043 (1,4)	0.835 (1,4)	0.802 (1,4)	0.678 (1,4)	1.397 (1,3)	0.988 (1,4)
30°	0.969 (1,4)	0.796 (1,4)	0.743 (1,4)	0.641 (1,4)	1.305 (1,4)	0.950 (1,4)
40°	0.897 (1,4)	0.762 (1,4)	0.686 (1,4)	0.608(1,4)	1.212 (1,4)	0.917 (1,4)
45°	0.861 (1,3)	0.746 (1,4)	0.659 (1,3)	0.593 (1,4)	1.168 (1,3)	0.901 (1,4)
$T = 600$ (K)						
10°	1.061 (1,3)	0.809 (1,4)	0.815 (1,3)	0.670 (1,4)	1.429 (1,3)	0.943 (1,4)
20°	1.003 (1,3)	0.772 (1,4)	0.768 (1,3)	0.634 (1,4)	1.354 (1,3)	0.903 (1,4)
30°	0.936 (1,3)	0.739 (1,4)	0.714 (1,4)	0.602 (1,4)	1.269 (1,3)	0.886 (1,3)
40°	0.868 (1,3)	0.710 (1,4)	0.660 (1,3)	0.574 (1,4)	1.182 (1,3)	0.844 (1,4)
45°	0.836 (1,3)	0.697 (1,4)	0.634 (1,3)	0.561 (1,4)	1.141 (1,3)	0.832 (1,4)

Table 4 Variation of the magnitudes of T_{1cst}^{axbuc}, T_{1sdt}^{axbuc} and corresponding axial buckling modes for CNT-patterned cones without elastic foundation in thermal environments versus the angle α

α	$\overline{T}_{1cst}^{axbuc}(m,n)$ U	$\overline{T}_{1sdt}^{axbuc}(m,n)$	$\overline{T}_{1cst}^{axbuc}(m,n)$ O	$\overline{T}_{1sdt}^{axbuc}(m,n)$	$\overline{T}_{1cst}^{axbuc}(m,n)$ X	$\overline{T}_{1sdt}^{axbuc}(m,n)$
$T = 300$ (K), $K_w = K_p = 0$						
10°	1.024 (1,4)	0.825 (1,4)	0.763 (1,4)	0.631 (1,4)	1.405 (1,4)	1.017 (1,4)
20°	0.956 (1,4)	0.782 (1,4)	0.708 (1,4)	0.593 (1,4)	1.319 (1,4)	0.970 (1,4)
30°	0.881 (1,4)	0.739 (1,5)	0.648 (1,4)	0.556 (1,4)	1.224 (1,4)	0.921 (1,5)
40°	0.807 (1,4)	0.698 (1,5)	0.589 (1,4)	0.520 (1,4)	1.131 (1,4)	0.880 (1,5)
45°	0.772 (1,4)	0.681 (1,5)	0.561 (1,4)	0.504 (1,4)	1.087 (1,4)	0.862 (1,5)
$T = 400$ (K)						
10°	0.976 (1,4)	0.764 (1,4)	0.720 (1,4)	0.586 (1,4)	1.351 (1,4)	0.938 (1,4)
20°	0.914 (1,4)	0.726 (1,4)	0.670 (1,4)	0.552 (1,4)	1.271 (1,4)	0.897 (1,4)
30°	0.844 (1,4)	0.687 (1,5)	0.615 (1,4)	0.520 (1,4)	1.182 (1,4)	0.853 (1,5)
40°	0.776 (1,4)	0.652 (1,5)	0.561 (1,4)	0.489 (1,4)	1.095 (1,4)	0.818 (1,5)
45°	0.743 (1,4)	0.637 (1,5)	0.535 (1,4)	0.475 (1,4)	1.053 (1,4)	0.803 (1,5)
$T = 500$ (K)						
10°	0.934 (1,4)	0.701 (1,4)	0.681 (1,4)	0.540 (1,4)	1.305 (1,4)	0.856 (1,4)
20°	0.877 (1,4)	0.668 (1,4)	0.636 (1,4)	0.511 (1,4)	1.231 (1,4)	0.820 (1,5)
30°	0.812 (1,4)	0.634 (1,5)	0.586 (1,4)	0.484 (1,5)	1.148 (1,4)	0.783 (1,5)
40°	0.749 (1,4)	0.605 (1,5)	0.536 (1,4)	0.457 (1,5)	1.065 (1,4)	0.754 (1,5)
45°	0.719 (1,4)	0.592 (1,5)	0.513 (1,4)	0.446 (1,5)	1.027 (1,4)	0.742 (1,5)
$T = 600$ (K)						
10°	0.894 (1,4)	0.632 (1,4)	0.643 (1,4)	0.492 (1,4)	1.263 (1,4)	0.765 (1,4)
20°	0.841 (1,4)	0.605 (1,5)	0.602 (1,4)	0.468 (1,4)	1.194 (1,4)	0.733 (1,5)
30°	0.782 (1,4)	0.575 (1,5)	0.557 (1,4)	0.443 (1,5)	1.116 (1,4)	0.704 (1,5)
40°	0.724 (1,4)	0.552 (1,5)	0.513 (1,4)	0.421 (1,5)	1.039 (1,4)	0.681 (1,5)
45°	0.697 (1,4)	0.542 (1,5)	0.491 (1,4)	0.412 (1,5)	1.003 (1,4)	0.672 (1,5)

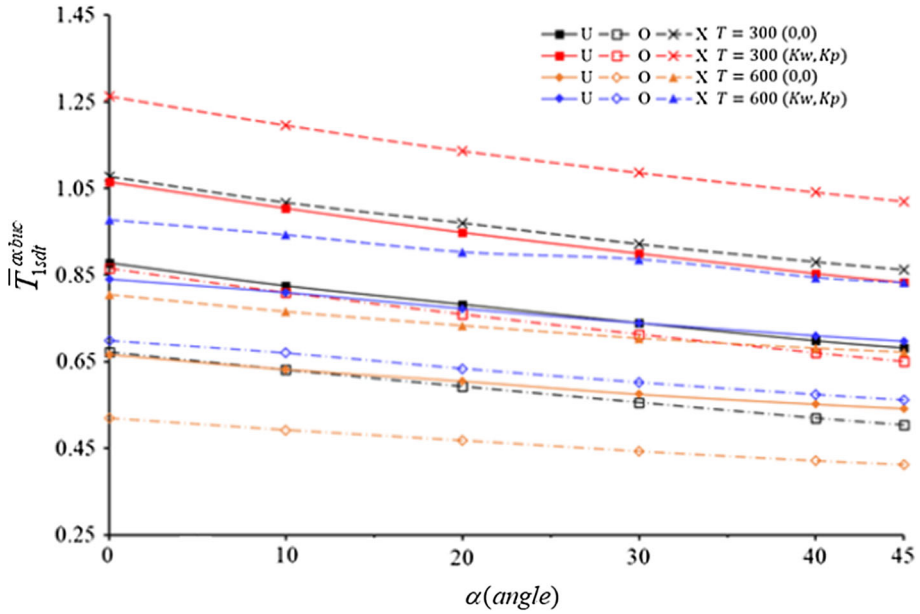

Fig. 3 Variation of NABLs for CNT-patterned conical shells with and without Pasternak elastic foundation versus the half-peak angle α with $T = 300$ and 600 (K) based on the SDT

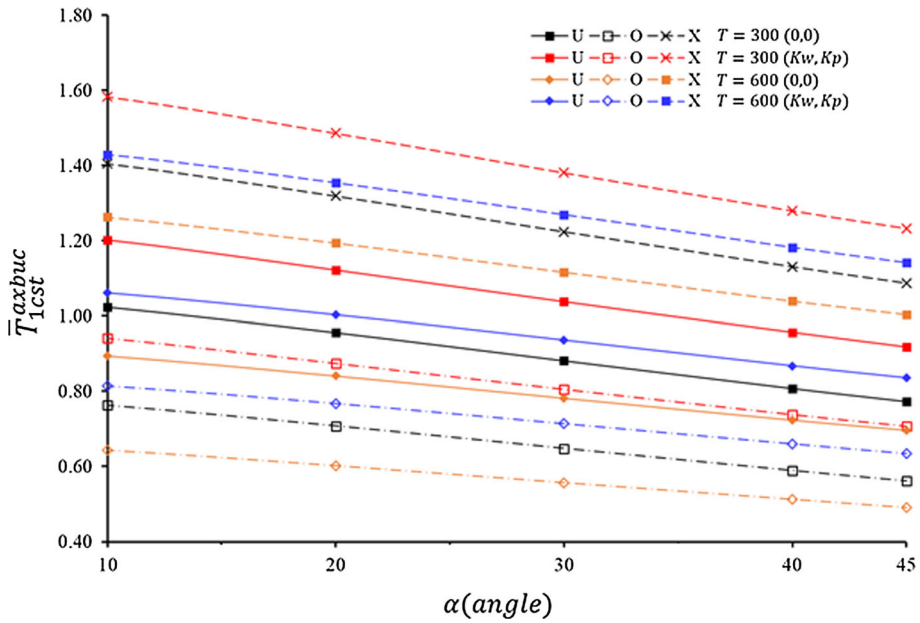

Fig. 4 Variation of NABLs for CNT-patterned conical shells with and without Pasternak elastic foundation versus the half-peak angle α with $T = 300$ and 600 (K) based on the CST

With an increase in α from 10° to 45°, the effect of TSDs on the values of the NABL decreases. In addition, although the influence of the soil reduces the influence of TSDs on the axial buckling load, on the contrary, the presence of the thermal environment makes it much more pronounced (see Figs. 3 and 4). For example, when $T = 300$ (K) and α increases from 10° to 45°, the influences of TSDs on the NABL for U-, O- and X-templates reduce from 16.47%, 14.03%, and 24.51% up to 9.37%, 8.06%, and 17.27%, respectively. At $T = 600$(K) and α increasing from 10° to 45°, the effect of transverse shear deformations on the NABL decreases from 23.75%, 17.79%, and 34.01% up to 16.63%, 11.51%, and 27.08% for U-, O-, and X-configurations, respectively.

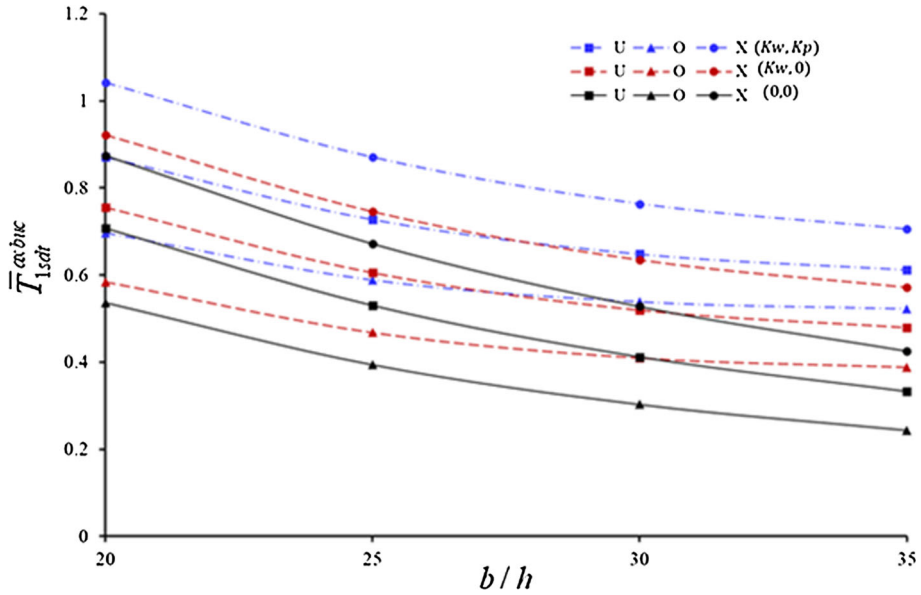

Fig. 5 Variation of NABLs of CNT-patterned conical shells with and without elastic foundations versus the b/h ratio within SDT at $T = 400$ (K)

It is noticed that the effects of O- and X-shapes on the NABL increase in comparison with the uniform distribution of CNTs when the half-peak angle increases. Furthermore, the ground effect reduces the influence of patterns on the magnitudes of axial buckling load, while the effect of thermal environment reduces the influence of the patterns. For example, when $T = 300$(K) and α increases from 10° to 45°, the effects of O- and X -patterns on the NABL compared to the uniform distribution are increasing from (− 19.42%) and (+ 19.02%) up to (− 21.88%) and (+ 22.6%), respectively, within the SDT. If $T = 600$(K) and α increases from 10° to 45°, the effects of O- and X-patterns on the NABL are increased from (− 17.18%) and (+ 16.56%) up to (− 19.51%) and (+ 19.37%), respectively. In addition, considering the TSDs reduce the pattern effects on the NABL compared to the CST. As the half-peak angle α increases, the influence of the elastic foundation on the NABL of CNT-patterned conical shells within SDT increases, although not significantly (by around 1%).

The variations of the NABL of CNT-patterned cones with the temperature-dependent material properties ($T = 400$ K) versus the b/h ratio for $(K_w,\ K_p) = (1.5 \times 10^8, 2.25 \times 10^4)$, $(K_w,\ K_p) = (1.5 \times 10^8, 0)$, and $(K_w,\ K_p) = (0, 0)$ based on SDT and CST are illustrated in Figs. 5 and 6, respectively. Other data are given as: $l/b = 1,\ V^*_{cnt} = 0.12,\ h = 0.002$ m and $T = 400$(K). In the presence of Pasternak and Winkler soils, the influence of TSDs on the NABLs with the increasing b/h ratio decreases significantly for all patterns, whereas it is more evident for the cone with the U-pattern. For instance, in the presence of Pasternak soil, the effects of TSDs on the NABLs in U-, O-, and X-patterned cones for $b/h = 20$ are 16.76%, 13.65%, and 25.44%, respectively, while for $b/h = 35$ those decrease up to 1.66%, 3.45%, and 4.33%, respectively. It is seen that those effects are more pronounced by around 0.58–2.25% in the presence of Winkler foundation and around 2–3% in the absence of the foundation.

In the grounded and ungrounded cases, as the b/h ratio increases, the influences of O- and X -patterns on NABLs are significantly reduced compared to the U-pattern in the framework of SDT, while those are more pronounced in the context of CST. For instance, in the framework of SDT and in the presence of the Pasternak foundation, the effects of O- and X-patterns on the NABL are (− 20.26%) and (+ 20.14%) for $b/h = 20$ and those are (− 14.89%) and (+ 15.91%) for $b/h = 35$. It has been determined that those effects are more pronounced by around 2–4% in the presence of the Winkler soil and by around 4–12% in the absence of the soil. In the framework of both theories, the foundation effect on the NABL increases strongly with the increase in the b/h ratio. Consider the TSD makes the ground effect on the NABL more pronounced than the CST, and it increases when the b/h ratio increases. It is revealed that the most significant effect of Pasternak and Winkler soils on the NABL is in the O-patterned cones. The small changes of the b/h ratio significantly increase the influence of the soils on the NABL.

The variation of the critical temperature of CNT-patterned conical shells (material properties independent of the temperature) with and without elastic foundations versus the V^*_{cnt} is given in Table 5. The data used

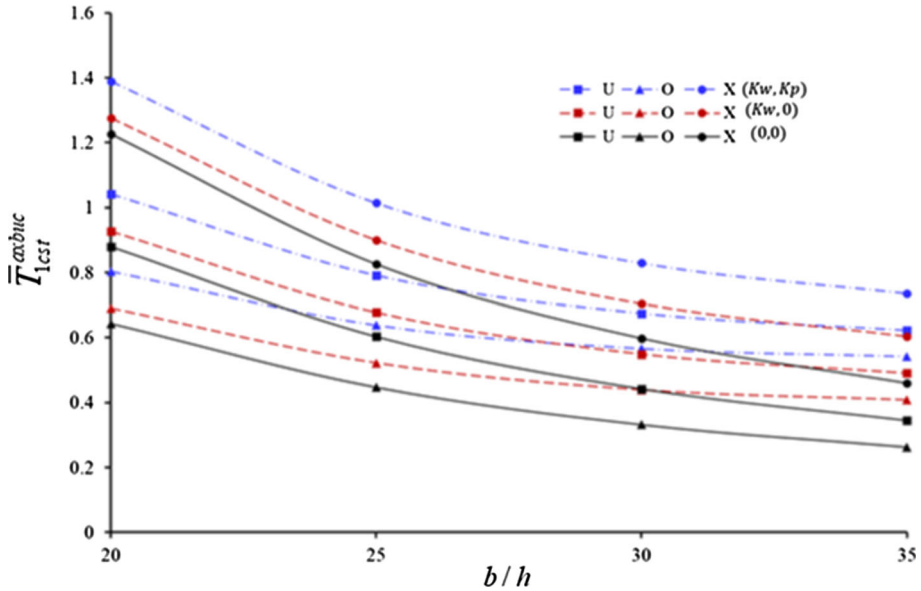

Fig. 6 Variation of NABLs of CNT-patterned conical shells with and without elastic foundations versus the b/h within CST at $T = 400$ (K)

Table 5 Variation of the critical temperature and corresponding modes (m, n) of CNT-patterned conical shells with and without elastic foundations versus the V_{cnt}^*

	T_{1cst}^{Tcrwp} (m, n) U	T_{1sdt}^{Tcrwp} (m, n)	T_{1cst}^{Tcrwp} (m, n) O	T_{1sdt}^{Tcrwp} (m, n)	T_{1cst}^{Tcrwp} (m, n) X	T_{1sdt}^{Tcrwp} (m, n)
V_{cnt}^*	$(K_w, K_P) = (1.5 \times 10^8, 2.75 \times 10^4)$					
0.12	1.080 (1,4)	0.923 (1,4)	0.840 (1,4)	0.736 (1,4)	1.434 (1,4)	1.110 (1,4)
0.17	1.545 (1,4)	1.342 (1,4)	1.192 (1,4)	1.051 (1,4)	2.071 (1,4)	1.636 (1,4)
0.28	2.236 (1,4)	1.798 (1,4)	1.686 (1,4)	1.440 (1,4)	3.116 (1,4)	2.159 (1,4)
V_{cnt}^*	$(K_w, K_P) = (0, 0)$					
0.12	0.919 (1,4)	0.761 (1,4)	0.678 (1,4)	0.574 (1,4)	1.272 (1,4)	0.945 (1,5)
0.17	1.384 (1,4)	1.181 (1,4)	1.031 (1,4)	0.890 (1,4)	1.910 (1,4)	1.474 (1,5)
0.28	2.074 (1,4)	1.633 (1,5)	1.525 (1,4)	1.279 (1,4)	2.955 (1,4)	1.990 (1,5)

in numerical calculations are: $T = 300\,(\mathrm{K})$, $l/b = 1$, $b/h = 20$, $K_w = 1.5 \times 10^8 (\mathrm{N/m^3})$, $K_P = 2.75 \times 10^4\,(\mathrm{N/m})$, $h = 0.002(\mathrm{m})$, $\alpha = 25°$. The influence of TSDs on the CT for CNT-patterned cones is significant but irregular as V_{cnt}^* increases. For example, while the effect of TSDs on the CT for cones with and without elastic foundations first increases and then decreases in all patterns. The highest effect of TSDs on the CT is found to be 32.66% in the X-patterned cone without elastic foundation at $V_{cnt}^* = 0.28$, while in the presence of the foundation it is 1.95% less. In the presence of the ground, when O- and X-patterns are compared with the U-pattern, the lowest effect on the CT within SDT is (-19.91%) for $V_{cnt}^* = 0.28$ in the O-pattern, while the largest effect occurs in the X-pattern with (+ 21.91%) for $V_{cnt}^* = 0.17$ in the framework of SDT. It is observed that the effect of soil on the CT decreases significantly when the volume fraction increases in the framework of both theories. For example, in the framework of SDT, at $V_{cnt}^* = 0.12$, 0.17, and 0.28, the ground effects on the CT of the O-patterned cones are 28.22%, 18.09%, and 12.59%, respectively, while those effects on the CT of the X-patterned cones are 17.46%, 10.99%, and 8.49%, respectively. In addition, it is determined that the effect of the foundation on the CT is about 2–5% more pronounced within SDT than the effect in the framework of CST.

5 Conclusions

Buckling of CNT-patterned conical shells under mechanical and thermal loads is carried out within SDT on the elastic foundations and in thermal environments. By using Donnell shell theory, basic equations of CNT-patterned truncated conical shells with temperature-dependent material properties are derived, and then analytical expressions are found for the axial buckling load and critical temperature of CNT-patterned conical shells under freely supported boundary conditions in elastic and thermal environments, using the Galerkin method. After confirming the accuracy of the obtained expressions with comparisons, the influences of the elastic foundation and thermal environment on the buckling behaviors are evaluated by changing the CNT patterns, volume fraction index, and parameters of the cone.

Appendix 1

The shear deformation theory proposed by Ambartsumian is built on the following assumptions [31]:

$$e_{33} = 0,\ \sigma_{13} = \frac{\mathrm{d}f_1}{\mathrm{d}z}\chi_1(S,\theta_1),\ \sigma_{23} = \frac{\mathrm{d}f_2}{\mathrm{d}z}\chi_2(S,\theta_1). \tag{19}$$

In the presence of a temperature field, the constitutive relations of CNT-patterned conical shells are formed as follows within SDT [15, 35]:

$$\begin{bmatrix}\tau_{11}\\ \tau_{22}\\ \tau_{12}\\ \tau_{13}\\ \tau_{23}\end{bmatrix} = \begin{bmatrix} H_{11}(z_1,T) & H_{12}(z_1,T) & 0 & 0 & 0\\ H_{21}(z_1,T) & H_{22}(z_1,T) & 0 & 0 & 0\\ 0 & 0 & H_{66}(z_1,T) & 0 & 0\\ 0 & 0 & 0 & H_{44}(z_1,T) & 0\\ 0 & 0 & 0 & 0 & H_{55}(z_1,T)\end{bmatrix}\begin{bmatrix}e_{11}\\ e_{22}\\ \gamma_{12}\\ \gamma_{13}\\ \gamma_{23}\end{bmatrix} + \begin{bmatrix}\tau_{11T}\\ \tau_{22T}\\ 0\\ 0\\ 0\end{bmatrix} \tag{20}$$

where τ_{ij} and $e_{ii}, \gamma_{ij} (i = 1, 2,\ j = 2, 3)$ are stresses and strains, respectively, and $H_{ij} (i, j = 1, 2, \ldots, 6)$ are defined as:

$$\begin{aligned} &H_{11}(z_1,T) = \frac{E_{11}(z_1,T)}{1-\nu_{12}\nu_{21}},\quad H_{12}(z_1,T) = \frac{\nu_{21}E_{11}(z_1,T)}{1-\nu_{12}\nu_{21}},\quad H_{21}(z_1,T) = \frac{\nu_{12}E_{22}(z_1,T)}{1-\nu_{12}\nu_{21}},\\ &H_{22}(z_1,T) = \frac{E_{22}(z_1,T)}{1-\nu_{12}\nu_{21}}, H_{44}(z_1,T) = G_{23}(z_1,T),\quad H_{55}(z_1,T) = G_{13}(z_1,T),\\ &H_{66}(z_1,T) = G_{12}(z_1,T) \end{aligned} \tag{21}$$

in which the thermal stresses τ_{11T} and τ_{22T} are defined as

$$\tau_{11T} = -H_{11}(z_1,T)\alpha_{11}(z_1,T)T(z_1),\ \tau_{22T} = -H_{22}(z_1,T)\alpha_{22}(z_1,T)T(z_1). \tag{22}$$

By using relations (19) and (20), the components of the strain field $(e_{11}, e_{22}, \gamma_{12})$ at an arbitrary point of the CNT-patterned conical shells can be expressed as those of its mid-surface $(e_{011}, e_{022}, \gamma_{012})$ and its curvature changes as follows:

$$\begin{bmatrix}e_{11}\\ e_{22}\\ \gamma_{12}\end{bmatrix} = \begin{bmatrix} e_{011} - z\dfrac{\partial^2 w}{\partial S^2} + I_1(z,T)\dfrac{\partial\chi_1}{\partial S}\\ e_{022} - \dfrac{z}{S^2}\dfrac{\partial^2 w}{\partial\theta_1^2} + \dfrac{1}{S}\dfrac{\partial w}{\partial S} + \dfrac{I_2(z,T)}{S}\dfrac{\partial\chi_2}{\partial\theta_1}\\ \gamma_{012} - 2z\left(\dfrac{1}{S}\dfrac{\partial^2 w}{\partial S\partial\theta_1} - \dfrac{1}{S^2}\dfrac{\partial w}{\partial\theta_1}\right) + \dfrac{I_2(z,T)}{S}\dfrac{\partial\chi_1}{\partial\theta_1} + I_1(z,T)\dfrac{\partial\chi_2}{\partial S}\end{bmatrix} \tag{23}$$

where

$$I_1(z,T) = \int_0^z \frac{\mathrm{d}f_1}{\mathrm{d}z}\frac{1}{G_{13}(z_1,T)}\mathrm{d}z,\quad I_2(z,T) = \int_0^z \frac{\mathrm{d}f_2}{\mathrm{d}z}\frac{1}{G_{23}(z_1,T)}\mathrm{d}z. \tag{24}$$

The forces $T_{ij}(i, j = 1, 2)$, $Q_i(i = 1, 2)$ and moments $M_{ij}(i, j = 1, 2)$ are obtained by integrating (20) through the thickness of CNT-reinforced cones [36, 37]:

$$\left(T_{ij},\ Q_i,\ M_{ij}\right) = \int_{-h/2}^{h/2} \left(\tau_{ij}, \tau_{i3}, \tau_{ij}z\right)dz,\quad (i, j = 1, 2), \tag{25}$$

Thermal forces $T_{11}^T,\ T_{22}^T$ and moments $M_{11}^T,\ M_{22}^T$ are expressed as follows:

$$\begin{aligned}
T_{11}^T &= \int_{-h/2}^{h/2} [H_{11}(z_1, T)\alpha_{11}(z_1, T) + H_{12}(z_1, T)\alpha_{22}(z_1, T)]\Delta T\,\mathrm{d}z,\\
T_{22}^T &= \int_{-h/2}^{h/2} [H_{21}(z_1, T)\alpha_{11}(z_1, T) + H_{22}(z_1, T)\alpha_{22}(z_1, T)]\Delta T\,\mathrm{d}z,\\
M_{11}^T &= \int_{-h/2}^{h/2} [H_{11}(z_1, T)\alpha_{11}(z_1, T) + H_{12}(z_1, T)\alpha_{22}(z_1, T)]\Delta T z\,\mathrm{d}z,\\
M_{22}^T &= \int_{-h/2}^{h/2} [H_{21}(z_1, T)\alpha_{11}(z_1, T) + H_{22}(z_1, T)\alpha_{22}(z_1, T)]\Delta T z\,\mathrm{d}z.
\end{aligned} \tag{26}$$

Appendix 2

The coefficients $b_{ij},\ c_{ij}\ (1, 2, \ldots, 4)$ and $I_j(j = 3, 4)$ in Eqs. (7)–(10) are expressed as

$$\begin{aligned}
&c_{11} = q_{11}^1 b_{11} + q_{12}^1 b_{21},\ c_{12} = q_{11}^1 b_{12} + q_{12}^1 b_{22},\ c_{13} = q_{11}^1 b_{13} + q_{12}^1 b_{23} + q_{11}^2,\\
&c_{14} = q_{11}^1 b_{14} + q_{12}^1 b_{24} + q_{12}^2,\ c_{15} = q_{11}^1 b_{15} + q_{12}^1 b_{25} + q_{15}^1, c_{18} = q_{11}^1 b_{18} + q_{12}^1 b_{28} + q_{18}^1,\\
&c_{21} = q_{21}^1 b_{11} + q_{22}^1 b_{21}, c_{22} = q_{21}^1 b_{12} + q_{22}^1 b_{22},\ c_{23} = q_{21}^1 b_{13} + q_{22}^1 b_{23} + q_{21}^2,\\
&c_{24} = q_{21}^1 b_{14} + q_{22}^1 b_{24} + q_{22}^2,\ c_{25} = q_{21}^1 b_{15} + q_{22}^1 b_{25} + q_{25}^1,\ c_{28} = q_{21}^1 b_{18} + q_{22}^1 b_{28} + q_{28}^1,\\
&c_{31} = q_{66}^1 b_{31},\ c_{32} = q_{66}^1 b_{32} + 2q_{66}^2,\ c_{35} = q_{35}^1 - q_{66}^1 b_{35},\ c_{38} = q_{38}^1 - q_{66}^1 b_{38},\\
&b_{11} = \frac{q_{22}^0}{\Delta},\ b_{12} = -\frac{q_{12}^0}{\Delta},\ b_{13} = \frac{q_{12}^0 q_{21}^1 - q_{11}^1 q_{22}^0}{\Delta},\ b_{14} = \frac{q_{12}^0 q_{22}^1 - q_{12}^1 q_{22}^0}{\Delta},\\
&b_{15} = \frac{q_{25}^0 q_{12}^0 - q_{15}^0 q_{22}^0}{\Delta},\ b_{18} = \frac{q_{28}^0 q_{12}^0 - q_{18}^0 q_{22}^0}{\Delta},\ b_{21} = -\frac{q_{21}^0}{\Delta};\ b_{22} = \frac{q_{11}^0}{\Delta},\\
&b_{23} = \frac{q_{11}^1 q_{21}^0 - q_{21}^1 q_{11}^0}{\Delta},\ b_{24} = \frac{q_{12}^1 q_{21}^0 - q_{22}^1 q_{11}^0}{\Delta},\ b_{25} = \frac{q_{15}^0 q_{21}^0 - q_{25}^0 q_{11}^0}{\Delta},\ b_{31} = \frac{1}{q_{66}^0},\\
&b_{28} = \frac{q_{18}^0 q_{21}^0 - q_{28}^0 q_{11}^0}{\Delta},\ \Delta = q_{11}^0 q_{22}^0 - q_{12}^0 q_{21}^0,\ b_{32} = -\frac{2q_{66}^1}{q_{66}^0},\ b_{35} = \frac{q_{35}^0}{q_{66}^0}, b_{38} = \frac{q_{38}^0}{q_{66}^0},\\
&I_3 = \int_{-h/2}^{h/2} \frac{\mathrm{d}f_1(z)}{\mathrm{d}z}\mathrm{d}z,\ I_4 = \int_{-h/2}^{h/2} \frac{\mathrm{d}f_2(z)}{\mathrm{d}z}\mathrm{d}z
\end{aligned} \tag{27}$$

in which $q_{ij}^{k_m}(m = 1, 2)$ are described by

$$q_{11}^{k_1} = \int_{-h/2}^{h/2} H_{11}(z_1, T)z^{k_1}\mathrm{d}z,\ q_{12}^{k_1} = \int_{-h/2}^{h/2} H_{12}(z_1, T)z^{k_1}\mathrm{d}z = \int_{-h/2}^{h/2} H_{21}(z_1, T)z^{k_1}\mathrm{d}z = q_{21}^{k_1},$$

$$q_{22}^{k_1} = \int_{-h/2}^{h/2} H_{22}(z_1, T) z^{k_1} \mathrm{d}z, \quad q_{66}^{k_1} = \int_{-h/2}^{h/2} H_{66}(z_1, T) z^{k_1} \mathrm{d}z\,; \quad k_1 = 0,\ 1,\ 2,$$

$$q_{15}^{k_2} = \int_{-h/2}^{h/2} z^{k_2} I_1(z, T) H_{11}(z_1, T) \mathrm{d}z, \quad q_{18}^{k_2} = \int_{-h/2}^{h/2} z^{k_2} I_2(z, T) H_{12}(z_1, T) \mathrm{d}z,$$

$$q_{25}^{k_2} = \int_{-h/2}^{h/2} z^{k_2} I_1(z, T) H_{21}(z_1, T) \mathrm{d}z, \quad q_{28}^{k_2} = \int_{-h/2}^{h/2} z^{k_2} I_2(z, T) H_{22}(z_1, T) \mathrm{d}z,$$

$$q_{35}^{k_2} = \int_{-h/2}^{h/2} z^{k_2} I_1(z, T) H_{66}(z_1, T) \mathrm{d}z, \ q_{38}^{k_2} = \int_{-h/2}^{h/2} z^{k_2} I_2(z, T) H_{66}(z_1, T) \mathrm{d}z, \ k_2 = 0, 1. \tag{28}$$

Appendix 3

The coefficients $u_{ij}(i, j = 1, 2, \ldots, 4)$ and u_T, u_W, u_P are described by

$$\begin{aligned}
u_{11} = &-\frac{2\delta_{-1}}{S_2^3}\left\{c_{12}\left[3(\xi-1)(\xi+1)^3 + 2\beta_1^2(\xi+4)(\xi+1) - \beta_1^4\right] - (c_{11}-c_{31})\beta_2^2\left(\xi^2 - \xi - 2 + \beta_1^2\right)\right\} \\
&- \frac{\delta_{-1}}{S_2^3}\left\{3(2c_{31}+c_{21}-3c_{11})\beta_2^2 + (c_{11}-5c_{12}-c_{22})\left[(\xi+1)^2(4\xi-5) + \beta_1^2(4\xi+7)\right]\right. \\
&\left.+2(7c_{12}+4c_{22}-4c_{11}-c_{21})\left[\left(\xi^2-\xi-2\right) + \beta_1^2\right] - 9(c_{11}-c_{12}-c_{22}+c_{21})\right\}, \\
u_{12} = &-\frac{2\delta_{-2}}{S_2^4}\left\{-c_{13}\left[(3\xi-4)\xi^3 + 2\xi(\xi+2)\beta_1^2 - \beta_1^4\right] + (c_{14}+c_{32})\beta_2^2\left[\xi(\xi-2) + \beta_1^2\right]\right. \\
&+ (4c_{14}+4c_{32}+c_{24})\beta_2^2 + (c_{23}+5c_{13}-c_{14})\left(2\xi^3 + 2\xi\beta_1^2 - 3\xi^2 + \beta_1^2\right) \\
&\left.+(4c_{14}-4c_{23}-7c_{13}+c_{24})\left[\xi(\xi-2) + \beta_1^2\right] - 3(c_{14}+c_{24}+c_{32})\beta_2^2 - 3(c_{23}+c_{13}-c_{14}-c_{24})\right\}, \\
u_{13} = &\frac{\delta_{-1}}{\beta_1 S_2^3}\left\{c_{35}\left[(2\xi-1)\xi + 2\beta_1^2\right]\beta_2^2 - c_{15}\left[(2\xi-1)\xi^3 + 3\xi\beta_1^2 - 2\beta_1^4\right] + 2c_{15} + c_{25}\right) \\
&\times\left(\beta_1^2 - \xi^2 + 2\xi^3 + 2\xi\beta_1^2\right) - 2c_{25}\left[(2\xi-1)\xi + 2\beta_1^2\right]\right\} \\
&- \frac{\delta_{+1}}{\beta_1 S_2^3}\left\{-I_3\left[\xi(1+2\xi) + 2\beta_1^2\right]S_2^2 + c_{35}(2\xi+1)\beta_2^2\right\}, \\
u_{14} = &\frac{\delta_{-1}\beta_2}{\beta_1^2 S_2^3}\left\{-2(c_{38}+c_{18})\beta_1^2\left[(\xi-1)\xi + \beta_1^2\right] - (c_{28}+2c_{18}+2c_{38})\beta_1^2 + 4c_{28}\beta_1^2\right\}, \\
u_{21} = &\frac{2\beta_2^2\delta_0}{S_2^2}\left[c_{21}\beta_2^2 + (c_{22}-c_{31})\left(\xi^2 - 1 + \beta_1^2\right) - c_{31} + c_{22} - c_{21}\right], \\
u_{22} = &-\frac{2\beta_2^2\delta_{-1}}{S_2^3}\left\{-2(c_{32}+c_{23})\left[(\xi-1)\xi + \beta_1^2\right] - 2c_{24}\beta_2^2 - c_{32} - c_{23} + c_{24}\right\}, \\
u_{23} = &\beta_2^2\left\{\frac{\delta_{-1}(c_{25}+c_{35})\left[(2\xi-1)\xi + 2\beta_1^2\right]}{S_2^3\beta_1} + \frac{2c_{35}\delta_0}{\beta_1 S_2^2}\right\}, \\
u_{24} = &-\frac{2\beta_2}{S_2^2}\left\{\left[c_{38}\left(\beta_1^2 + \xi^2\right) + c_{28}\beta_2^2\right]\delta_0 + I_4\delta_{+2}\right\}, \\
u_{31} = &\frac{2\delta_{-1}}{S_2^3}\left\{b_{11}\beta_2^4 + (b_{31}+b_{21}+b_{12})\beta_2^2\left(\xi^2 - 1 + \beta_1^2\right) + (2b_{31}+3b_{21}+b_{12})\beta_2^2 - (b_{31}+2b_{21}+2b_{11})\beta_2^2\right. \\
&\left.+ b_{22}\left[\beta_1^4 - (\xi+1)^3(3\xi-1) - 2(\xi+3)(\xi+1)\beta_1^2\right] + (4b_{22}+b_{12}-b_{21})\left(2\beta_1^2\xi - 1 + 3\xi^2 + 3\beta_1^2 + 2\xi^3\right)\right.
\end{aligned}$$

$$
\begin{aligned}
&-(5b_{22}+3b_{12}-3b_{21}-b_{11})\left(\beta_1^2+\xi^2-1\right)+2(b_{11}+b_{21}-b_{22}-b_{12})\big\},\\
u_{32} &= -\frac{\delta_{-1}}{S_2^4}\big\{-2b_{14}\beta_2^4+2(b_{32}-b_{13}-b_{24})\left(\xi^2-\xi+\beta_1^2\right)-(b_{13}-2b_{32}+3b_{24})\beta_2^2-2(b_{32}-2b_{24}-2b_{14})\beta_2^2\\
&\quad-2b_{23}\left[(2-3\xi)\xi^3-2\beta_1^2\xi(\xi+1)+\beta_1^4\right]-(b_{13}-b_{24}+4b_{23})\left(4\xi^3-3\xi^2+4\beta_1^2\xi+\beta_1^2\right)\\
&\quad-2(b_{14}-3b_{13}+3b_{24}-5b_{23})\left[\xi^2-\xi+\beta_1^2\right]+(b_{14}-3b_{13}+3b_{24}-5b_{23})\big\}+\frac{2\delta_0(\beta_1^2+\xi^2)}{S_2^3}\cot\alpha,\\
u_{33} &= \frac{2\delta_0\left(\beta_1^2+\xi^2\right)}{\beta_1 S_2^3}\left[(b_{35}+b_{15})\beta_2^2-b_{25}\left(\xi^2-\beta_1^2\right)-(b_{25}+b_{15})\xi-b_{15}\right],\\
u_{34} &= \frac{2\delta_0}{S_2^3}\left[b_{18}\beta_2-b_{18}\beta_2^3-(b_{38}+b_{28})\beta_2\left(\beta_1^2+\xi^2\right)\right],\\
u_{41} &= -\frac{2\delta_0\left(\beta_1^2+\xi^2\right)}{S_2^2}\cot\alpha,\quad u_{43}=-\frac{\delta_{+1}I_3}{\beta_1 S_2}\left[(2\xi+1)(1+\xi)+2\beta_1^2\right],\\
u_{44} &= \frac{2I_4\delta_{+1}\beta_2}{\beta_1 S_2},\quad u_T=-\frac{2(\xi^2+\beta_1^2)\delta_0}{S_2^2},\quad u_W=-2\delta_{+2}K_w,\quad u_P=-\frac{2\delta_0\left(\xi^2+\beta_1^2+\beta_2^2\right)}{S_2^2}K_p
\end{aligned}
\tag{29}
$$

where

$$
\delta_i=\frac{\beta_1^2\left[1-e^{-(2\xi+i)x_0}\right]}{\left[(2\xi+i)^2+4\beta_1^2\right](2\xi+i)};\ i=-2;-1;\ 0;\ 1;\ 2. \tag{30}
$$

References

1. Iijima, S., Ichihashi, T.: Single-shell carbon nanotubes of 1-nm diameter. Nature **363**, 603–605 (1993). https://doi.org/10.1038/363603a0
2. Lu, J.P.: Elastic properties of single and multilayered nanotubes. J. Phys. Chem. Solids **58**, 1649–1652 (1998). https://doi.org/10.1016/S0022-3697(97)00045-0
3. Krishnan, A., Dujardin, E., Ebbesen, T.W., Yianilos, P.N., Treacy, M.M.J.: Young's modulus of single-walled nanotubes. Phys. Rev. B Condens. Matter. **58**, 14013 (1998). https://doi.org/10.1103/PhysRevB.58.14013
4. Loos, M.: Carbon Nanotube Reinforced Composites. Elsevier Inc (2015). https://doi.org/10.1016/C2012-0-06123-6
5. Cantor, B., Allen, C.M., Dunin-Burkowski, R., Green, M.H., Hutchinson, J.L., O'Reilly, K.A., Perford-Long, A.K., Schumacher, P., Sloan, J., Warren, P.J.: Appl. Nanocompos. Scr. Mater. **44**(8–9), 2055–2090 (2001). https://doi.org/10.1016/S1359-6462(01)00891-0
6. Hussain, M.S., Al-Swailem, S., Hala, A.: Advanced nanocomposites for high temperature aero-engine/turbine components. Int. J. Nanomanuf. **4**(1–4), 248–256 (2009). https://doi.org/10.1504/IJNM.2009.028132
7. Wang, Z., Xiao, H.: Nanocomposites: recent development and potential automotive applications. SAE Int. J. Mater. Manuf. **1**(1), 631–640 (2009). https://doi.org/10.2307/26282698
8. Han, Z.D., Fina, A.: Thermal conductivity of carbon nanotubes and their polymer nanocomposites: a review. Prog. Polym. Sci. **36**, 914–944 (2011). https://doi.org/10.1016/j.progpolymsci.2010.11.004
9. Spitalsky, Z., Tasis, D., Papagelis, K., Galiotis, C.: Carbon nanotube-polymer composites: chemistry, processing, mechanical and electrical properties. Prog. Polym. Sci. **35**, 357–401 (2010). https://doi.org/10.1016/j.progpolymsci.2009.09.003
10. Kuilla, T., Bhadra, S., Yao, D.H., Kim, N.H., Bose, S., Lee, J.N.: Recent advances in graphene based polymer composites. Prog. Polym. Sci. **35**, 1350–1375 (2010). https://doi.org/10.1016/j.progpolymsci.2010.07.005
11. Fu, S., Sun, Z., Huang, P., Li, Y., Hu, N.: Some basic aspects of polymer nanocomposites: a critical review. Nano Mater. Sci. **1**(1), 2–30 (2019). https://doi.org/10.1016/j.nanoms.2019.02.006
12. Russo, P., Cimino, F., Tufano, A., Fabbrocino, F.: Thermal and quasi-static mechanical characterization of polyamide 6-graphene nanoplatelets composites. Nanomaterials **11**(6), 1454 (2021). https://doi.org/10.3390/nano11061454
13. Kwon, H., Bradbury, C.R., Leparoux, M.: Fabrication of functionally graded carbon nanotube-reinforced aluminum matrix composite. Adv. Eng. Mater. **13**, 325–329 (2011). https://doi.org/10.1002/adem.201000251
14. Shen, H.S.: Postbuckling of nanotube-reinforced composite cylindrical shells in thermal environments, Part I: axially-loaded shells. Compos. Struct. **93**, 2096–2108 (2011). https://doi.org/10.1016/j.compstruct.2011.02.011
15. Shen, H.S.: Thermal buckling and postbuckling behavior of functionally graded carbon nanotube-reinforced composite cylindrical shells. Compos. Part B Eng. **43**(3), 1030–1038 (2012). https://doi.org/10.1016/j.compositesb.2011.10.004
16. Shen, H.S., Xiang, Y.: Thermal buckling and postbuckling behavior of FG-GRC laminated cylindrical shells with temperature-dependent material properties. Meccanica **54**(1), 283–297 (2019). https://doi.org/10.1007/s11012-019-00945-0
17. Kiani, Y.: Buckling of functionally graded graphene reinforced conical shells under external pressure in thermal environment. Compos. Part B-Eng. **156**, 128–137 (2019). https://doi.org/10.1016/j.compositesb.2018.08.052
18. Mahani, R.B., Eyvazian, A., Musharavat, F., Sebaey, T.A., Talebizadehsardari, P.: Thermal buckling of laminated nanocomposite conical shell reinforced with graphene platelets. Thin-Walled Struct. **155**, 106913 (2020). https://doi.org/10.1016/j.tws.2020.106913

19. Shen, H.S., Xiang, Y., Reddy, J.N.: Assessment of the effect of negative Poisson's ratio on the thermal postbuckling of temperature dependent FG-GRMMC laminated cylindrical shells. Comput. Meth. Appl. Mech. Eng. **376**, 113664 (2021). https://doi.org/10.1016/j.cma.2020.113664
20. Pakravan, I., Heidari, S.A., Talebitooti, R., Talebitooti, M.: Haar wavelet technique applied on the functionally graded carbon nanotube reinforced conical shells to study free vibration and buckling behaviors in thermal environments. J. Vib. Control (2021). https://doi.org/10.1177/1077546321996931
21. Bacciocchi, M., Fantuzzi, N., Ferreira, A.J.M.: Static finite element analysis of thin laminated strain gradient nanoplates in hygro-thermal environment. Continuum Mech. Thermodyn. **4**(3), SI:969–992 (2021), doi:https://doi.org/10.1007/s00161-020-00940-x
22. Pasternak, P.L.: Design of Foundations on Elastic Bed: Fundamentals of a New Method Based on Two Moduli of Subgrade Reaction. Gosstroiizdat, Moscow (1954) (**in Russian**)
23. Sun, B., Huang, Y.: The exact solution for the general bending problems of conical shells on the elastic foundation. Appl. Math. Mech. Eng. Ed. **9**, 455–469 (1988). https://doi.org/10.1007/BF02465684
24. Sofiyev, A.H.: Thermal buckling of FGM shells resting on a two-parameter elastic foundation. Thin-Walled Struct. **49**, 1304–1311 (2011). https://doi.org/10.1016/j.tws.2011.03.018
25. Duc, N.D., Cong, P.H., Anh, V.M., Quang, V.D., Tran, P., Tuan, N.D., Thinh, N.H.: Mechanical and thermal stability of eccentrically stiffened functionally graded conical shell panels resting on elastic foundations and in thermal environment. Compos. Struct. **132**, 597–609 (2015). https://doi.org/10.1016/j.compstruct.2015.05.072
26. Sofiyev, A.H., Pirmamedov, I.T., Kuruoglu, N.: Influence of elastic foundations and carbon nanotube reinforcement on the hydrostatic buckling pressure of truncated conical shells. Appl. Math. Mech. (Eng. Ed.) **41**(7), 1011–1026 (2020), https://doi.org/10.1007/s10483-020-2631-7
27. Nam, V.H., Phuong, N.T., Duc, V.M.: Nonlinear buckling of orthogonal carbon nanotube-reinforced composite cylindrical shells under axial compression surrounded by elastic foundation in thermal environment. Int. J. Comput. Mater. Sci. Eng. **8**(4), 1950016 (2019). https://doi.org/10.1142/S2047684119500167
28. Hieu, P.T., Van Tung, H.: Thermal buckling and postbuckling of CNT-reinforced composite cylindrical shell surrounded by an elastic medium with tangentially restrained edges. J Thermoplastic Compos. Mater. **34**(7), 861–883 (2021). https://doi.org/10.1177/0892705719853611
29. Avey, M., Tornabene, F., Dimitri, R., Kuruoglu, N.: Free vibration of thin-walled composite shell structures reinforced with uniform and linear carbon nanotubes: effect of the elastic foundation and nonlinearity. Nanomaterials **11**(8), 2090 (2021). https://doi.org/10.3390/nano11082090
30. Babaei, H., Kiani, Y., Eslami, M.R.: Vibrational behavior of thermally pre-/post-buckled FG-CNTRC beams on a nonlinear elastic foundation: a two-step perturbation technique. Acta Mech. **232**, 3897–3915 (2021). https://doi.org/10.1007/s00707-021-03027-z
31. Ambartsumian, S.A.: Theory of Anisotropic Shells, NASA, TT F-118 (1964).
32. Tımarci, T., Soldatos, K.P.: Comparative dynamic studies for symmetrical cross-ply circular cylindrical-shells on the basis of a unified shear-deformable shell theory. J. Sound Vib. **187**, 609–624 (1995)
33. Reddy, J.N.: Mechanics of Laminated Composite Plates and Shells. Theory and Analysis, Boca Raton, CRC Press (2004).
34. Viola, E., Tornabene, F., Fantuzzi, N.: General higher-order shear deformation theories for the free vibration analysis of completely doubly-curved laminated shells and panels. Compos. Struct. **95**, 639–666 (2013). https://doi.org/10.1016/j.compstruct.2012.08.005
35. Sofiyev, A.H.: Thermoelastic stability of freely supported functionally graded conical shells within the shear deformation theory. Compos. Struct. **152**, 74–84 (2016). https://doi.org/10.1016/j.compstruct.2016.05.027
36. Agamirov, V.L.: Dynamic Problems of Nonlinear Shells Theory. Nauka, Moscow (1990). (**in Russian**)
37. Eslami, M.R.: Buckling and Postbuckling of Beams, Plates and Shells. Springer, Switzerland (2018)